Asymmetric beam-beam effect study in a highly polarized electron-ion collider

Ming Xuan Chang,[1,2] Jian Cheng Yang,[1,*] Lei Wang,[1,2] Jie Liu,[1] He Zhao,[1] Guo Dong Shen,[1] Hang Ren,[1,2] Yun Zhe Gao,[1,2] Qi Yu Kong,[1,2] Fu Ma,[1,2] and Min Xiang Li[3,1]

[1]*Institute of Modern Physics, Chinese Academy of Sciences, Lanzhou 730000, China*
[2]*University of Chinese Academy of Sciences, Beijing 100049, China*
[3]*Lanzhou University, Lanzhou 730000, China*

(Received 6 April 2022; accepted 15 December 2022; published 11 January 2023)

The EicC (The highly polarized Electron-ion collider in China) project proposes a scheme with different numbers of bunches in the two rings, which leads to an asymmetric beam-beam effect, also known as the gear-change effect. In order to investigate the feasibility of asymmetric collision in EicC, a self-consistent simulation program named AthenaGPU, which uses GPU for high-performance computing, was developed. A linearized matrix model is used to account for the dipole instability that occurs in the simulation. The simulation results in different collision modes show that asymmetric collision can lead to instability, and the beam can be stabilized by adjusting the nominal tunes. In the process of scanning the beam intensity, instability may occur as the beam intensity decreases, and this instability can be suppressed by compensating the nominal tunes. Offset collision simulations show that the decoherence time of the displaced bunch is shorter in the asymmetric collision than in the symmetric collision. The study in this paper suggests that asymmetric collision is promising for EicC when only the beam-beam effect is considered.

DOI: 10.1103/PhysRevAccelBeams.26.011001

I. INTRODUCTION

The highly polarized Electron-ion collider in China (EicC) is proposed by the Institute of Modern Physics, Chinese Academy of Sciences (IMP) with a center-of-mass energy of 15–20 GeV to study the structure of the nucleons [1]. EicC aims at a peak luminosity of 2.0×10^{33} cm^{-2} s^{-1} for electron-proton (e-p) collision, as well as ensuring an average polarization for electrons and protons of about 80% and 70%, respectively. In the proposed design of EicC, a figure-8 ion collider ring (pRing), a polarized electron injector, and a racetrack electron collider ring (eRing) will be constructed based on the HIAF project [2], as shown in Fig. 1. The existing HIAF-BRing can provide a polarized proton beam for the pRing. The electron injector provides the eRing with a polarized electron beam. Table I shows the main parameters required to reach the peak luminosity for e-p collision. EicC will only use one interaction point IP1 in the current design, and the other interaction point IP2 is reserved for future upgrades.

As shown in Table I, the number of electron and proton bunches in eRing and pRing is different. In this asymmetric collision mode, the beam-beam effect causes coupling between multiple bunches in the two rings. This coupling will introduce new resonances that do not occur in symmetric cases and then limit the choice of the nominal tunes. In this paper, all bunches in the two rings are assumed to be equally spaced, so for simplicity, the number of bunches in the two rings can be reduced to coprime. That is, the collisions between 256 electron bunches and 448 proton bunches are equivalent to the collisions between 4 electron bunches and 7 proton bunches. Past studies have shown that such an asymmetric design is not feasible if the least common multiple of the number of bunches in the two rings is large [3,4]. However, the value of the least common multiple in EicC is 28, which is not a large value. To investigate the feasibility of 4e vs 7p collision mode in

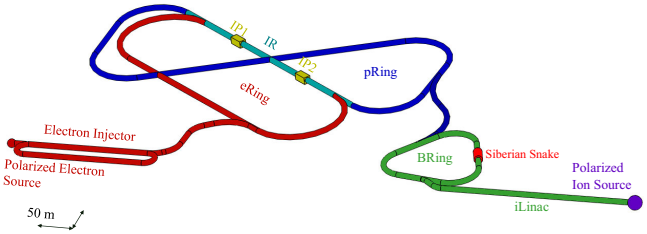

FIG. 1. The layout of the EicC.

*Corresponding author.
yangjch@impcas.ac.cn

TABLE I. The main parameters of the EicC.

Parameter	Electron	Proton
Circumference (m)	767.47	1341.59
Kinetic energy (GeV)	3.5	19.08
Collision frequency (MHz)	100	
Polarization	80%	70%
Particles per bunch (10^{11})	1.7	1.25
Number of bunches	256	448
β_x^*/β_y^* (m)	0.2/0.06	0.04/0.02
rms emittance (H/V) (nm)	60/60	300/180
rms bunch size (H/V) (μm)	110/60	
Transverse tune (H/V)	0.58/0.56	0.315/0.3
rms bunch length (m)	0.02	0.04
rms momentum spread	1.0×10^{-3}	6.5×10^{-4}
Synchrotron tune	0.025	0.01
Beam-beam parameter (H/V)	0.088/0.048	0.004/0.004
Crossing angle (mrad)	2×25	
Hourglass factor	0.788	
Transverse damping time (turns)	2000	∞
Longitudinal damping time (turns)	1000	∞
Luminosity ($\mathrm{cm}^{-2}\,\mathrm{s}^{-1}$)	2.0×10^{33}	

EicC, the circulant matrix method is used to construct a matrix for linearized analysis, and a self-consistent program is developed for simulation.

Self-consistent simulation is suitable for arbitrary particle distributions, but it is very time-consuming, so parallel algorithms are introduced to speed it up [5–7]. NVIDIA provides the cuFFT library [8], an efficient GPU-based (Graphics Processing Unit) Fast Fourier Transform library, which helps speed up computations when solving the field. In addition, the linear transfer of particles is of a single-instruction-multiple-data operation type, and the GPU can achieve a good acceleration effect for this operation. Therefore, a GPU-based self-consistent simulation program named AthenaGPU is developed using Cuda C++ language [9].

In this paper, simulation and matrix models are introduced in Sec. II. The impact of collision modes on beam stability is presented in Sec. III. The study of beam-beam limit is presented in Sec. IV. Simulations of the transverse offset due to a rapid disturbance are performed in Sec. V. Finally, a summary is presented in Sec. VI.

II. MODELS

A. The simulation model

In the case of asymmetric collisions, the beam with fewer bunches is called the basic beam, and the other beam is called the nonbasic beam. A superperiod is complete when all bunches of one beam have collided once with all bunches in the other beam. In a superperiod, the number of revolutions of the basic beam is called the basic turns, which is equal to the number of nonbasic bunches, and the concept of the nonbasic turns can be obtained in the same way. The parameters in Table I show that the electron beam is the basic beam, the proton beam is the nonbasic beam, 28 collisions occur in one superperiod, and the basic and nonbasic turns are 7 and 4, respectively.

The entire simulation is performed according to the following procedures.

1. Initialization

A macroparticle is described using charge, mass, phase space coordinates $(x, p_x, y, p_y, z, \delta_p)$, and a tag in the program. Here, x and y are transverse coordinates, p_x and p_y are transverse momenta normalized by the total momentum of the reference particle, z is the distance from the reference particle, and δ_p is the momentum deviation. A tag is a number greater than 0 and unique to each macroparticle so that a specific macroparticle can be tracked. When a macroparticle is lost, its tag is multiplied by -1, after which it will no longer participate in any calculations.

The program can generate particles that obey Gaussian, KV, or uniform distribution in the transverse direction and Gaussian distribution in the longitudinal direction [10,11]. These distributions can satisfy various simulation conditions. In this paper, the initial distributions of the bunches in the transverse direction are all Gaussian distributions.

2. Crossing angle

When there is a crossing angle between the two beams, the particles in the laboratory frames are transformed to the same boosted frame through Lorentz transformation, and then they can be treated as head-on collisions. An inverse Lorentz transformation is performed on the particles to bring them back to the laboratory frames when the

interactions in the collision region are complete. The transformation is well documented in Ref. [12]. EicC will use crab cavities to avoid the luminosity degradation caused by the crossing angle. This paper assumes that there is no crossing angle between the two beams moving in opposite directions, as the discussion about the crab cavity is beyond the scope of this paper.

3. Hourglass effect

The program performs a linear map for the revolutions and a stochastic map for synchrotron radiation damping and quantum excitation effects [13].

In the interaction region, the transverse distribution of the bunch undergoes an hourglass-like deformation, and this geometric effect leads to a degradation of luminosity. For two Gaussian bunches, the luminosity $\mathcal{L}$ is given by

$$\mathcal{L} = \frac{f_c N_e N_i}{2\pi\sqrt{(\sigma_{e_x}^2 + \sigma_{i_x}^2)(\sigma_{e_y}^2 + \sigma_{i_y}^2)}} R_h, \tag{1}$$

where the subscripts e and i are used to distinguish between electron and ion bunches, f_c is the collision frequency, N is the number of particles per bunch, and σ_x and σ_y are the horizontal and vertical bunch sizes at the IP. The hourglass reduction factor R_h is given by [14]

$$R_h = \int_{-\infty}^{+\infty} \frac{1}{\sqrt{\pi}} \frac{\exp(-t^2)}{\sqrt{(1 + t^2/t_x^2)(1 + t^2/t_y^2)}} dt, \tag{2}$$

$$t_u^2 = \frac{2(\sigma_{e_u}^2 + \sigma_{i_u}^2)}{(\sigma_{e_s}^2 + \sigma_{i_s}^2)(\sigma_{e_u}^2/\beta_{e_u}^2 + \sigma_{i_u}^2/\beta_{i_u}^2)}, \qquad u = x, y, \tag{3}$$

where β_x and β_y are the horizontal and vertical beta function at the IP, respectively, and σ_s is the bunch length.

The hourglass effect would couple the transverse and longitudinal oscillations, which may lead to synchrobetatron resonance. In order to accurately model the impact caused by the hourglass effect, a sufficient number of slices is required to make the result converge.

The transverse electric field is calculated by interpolation to reduce the number of slices [15]. The transverse electric field induced by the opposite slice and acting on the forward slice can be given by

$$E_{x,y}(s) = E_{x,y}(s_{\text{tail}}) + \frac{E_{x,y}(s_{\text{head}}) - E_{x,y}(s_{\text{tail}})}{s_{\text{head}} - s_{\text{tail}}}(s - s_{\text{tail}}), \tag{4}$$

$$E_{x,y}(s_{\text{head}}) = -\frac{\partial\phi(s_{\text{head}})}{\partial x, y}, \qquad E_{x,y}(s_{\text{tail}}) = -\frac{\partial\phi(s_{\text{tail}})}{\partial x, y}, \tag{5}$$

where s is the longitudinal position of the macroparticle in the forward slice that has drifted to the real collision point CP, s_{head} and s_{tail} are the longitudinal positions of the head and tail of the forward slice, as shown in Fig. 2. The opposite slice is transferred to s_{head} and s_{tail}, and then the potentials $\phi(s_{\text{head}})$ and $\phi(s_{\text{tail}})$ induced by the opposite slice are calculated by the particle-in-cell method.

The longitudinal electric field is given by

$$E_z = -\frac{\phi(s_{\text{head}}) - \phi(s_{\text{tail}})}{s_{\text{head}} - s_{\text{tail}}}. \tag{6}$$

In the process of solving the field by the interpolation method, if the number of slices of the two bunches involved in the collision is N_s^e and N_s^i, respectively, the Poisson equation needs to be solved $4N_s^e N_s^i$ times during one collision.

4. Field solver and one-turn map

The cloud-in-cell method [16] is used to project the macroparticles in a slice onto a two-dimensional mesh to obtain the transverse charge density distribution $\rho_{x,y}$, where x and y are grid coordinates. Macroparticles projected outside the mesh are considered lost.

This program uses the Green function to solve the Poisson equation under open boundary conditions. In order to reduce the error when the size of the grid is greatly different in the horizontal and vertical directions and to avoid the problem of the Green function having a singularity at $x^2 + y^2 = 0$, the Green function is replaced by the integral Green function [17]. The integral Green function is given by

$$\begin{aligned} G(x_j, y_k) &= -\frac{1}{2\pi\epsilon_0}\int_{x_j - h_x/2}^{x_j + h_x/2}\int_{y_k - h_y/2}^{y_k + h_y/2} \ln(x^2 + y^2)dxdy \\ &= -\frac{1}{2\pi\epsilon_0}\left[-3xy + x^2 \arctan\frac{y}{x} + y^2 \arctan\frac{x}{y} \right. \\ &\quad \left. + xy \ln(x^2 + y^2)\right]\Bigg|_{x_j - h_x/2}^{x_j + h_x/2}\Bigg|_{y_k - h_y/2}^{y_k + h_y/2}, \end{aligned} \tag{7}$$

where h_x and h_y are the horizontal and vertical sizes of the grid, respectively, ϵ_0 is the vacuum permittivity, and the subscripts j and k indicate the coordinates of the grid point in the mesh.

The momentum changes of the macroparticle due to the beam-beam kick are given by [13]

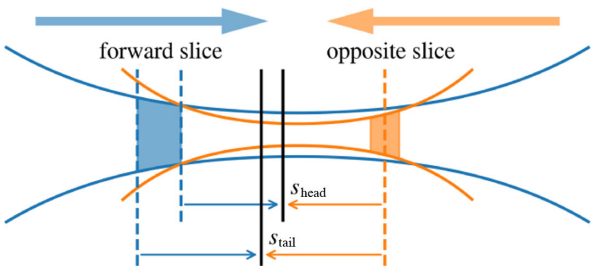

FIG. 2. Interpolation scheme of fields.

$$\Delta p_{e_x,e_y} = \frac{1+|\beta_e\beta_i|}{|\beta_e|+|\beta_i|}\frac{q_e E_{i_x,i_y}}{\gamma_e m_e c^2}, \tag{8}$$

$$\Delta p_{e_z} = \frac{1}{2}\Delta p_{e_x}\left(p_{e_x}+\frac{1}{2}\Delta p_{e_x}\right) + \frac{1}{2}\Delta p_{e_y}\left(p_{e_y}+\frac{1}{2}\Delta p_{e_y}\right) + \frac{1}{|\beta_e|+|\beta_i|}\frac{q_e E_{i_z}}{\gamma_e m_e c^2}, \tag{9}$$

where c is the speed of light, $\beta = v/c$, γ is the Lorentz factor, m and q are the rest mass and charge of the macroparticle, and E is the electric field. Usually, Δp_z can be ignored because its value is very small. The program provides an option to set whether to calculate the change of p_z. In the study of this paper, the change of p_z is not considered.

5. Parallelization

The program supports thread-level parallelism within a GPU and hardware-level parallelism across multiple GPUs. For a single GPU, thousands of Cuda cores can be called for computation simultaneously. If multiple GPUs are available, the program's scheduler will evenly allocate the basic bunches to each GPU. In each basic turn, the scheduler uses the Cuda streams to asynchronously copy the nonbasic bunches to the corresponding GPU to save the data transmission time, i.e., the program transfers data while performing calculations such as slicing on the basic bunches. Then each GPU starts to compute independently. The optimal acceleration effect can be achieved when the number of GPUs and basic bunches are the same. A parallel reduction algorithm is used to get bunch statistics such as centroid, size, etc., and calculate the luminosity.

The performance of the program is tested using a 512×512 mesh. In the case of 1 electron bunch colliding with 1 proton bunch and 10 slices per bunch, the computational speed of the program is shown in Fig. 3(a). K20m, K80, V100, and A100 are GPUs released in 2013, 2014, 2017, and 2020, respectively. When the number of macroparticles is $\lesssim 1 \times 10^6$, the limitation of the computational speed is mainly in the process of solving the field, i.e., the limitation of the clock frequency. When the number of macroparticles is 1×10^7 and 1×10^8, the limitation of the computational speed is mainly in the bunch slicing and hourglass process, that is, the bandwidth limitation. Since the memory required for the simulation exceeds the upper limit of K20m and K80 when the number of macroparticles is 1×10^8, only the results of V100 and A100 are shown at this point. The performance test results show that the hardware upgrades have effectively improved the simulation speed. Since GPU is still in rapid development, it is a good choice to develop a GPU-based simulation program. Figure 3(b) shows the computation speed of eight electron bunches colliding with nine proton bunches. Here, eight A100 GPUs are called for simulation. In the case of 1×10^6 macroparticles per bunch and 10 slices per bunch, the speedup is 6.8 compared to using only one GPU.

B. The matrix model

A matrix including betatron oscillation, synchrotron oscillation, hourglass effect, and asymmetric collision is constructed and then used to analyze the instability by the eigenvalues of the matrix. The details of using matrices to implement synchrotron oscillation and asymmetric collision are well described in Refs. [18] and [4], respectively, and a combination of the two approaches will be presented here.

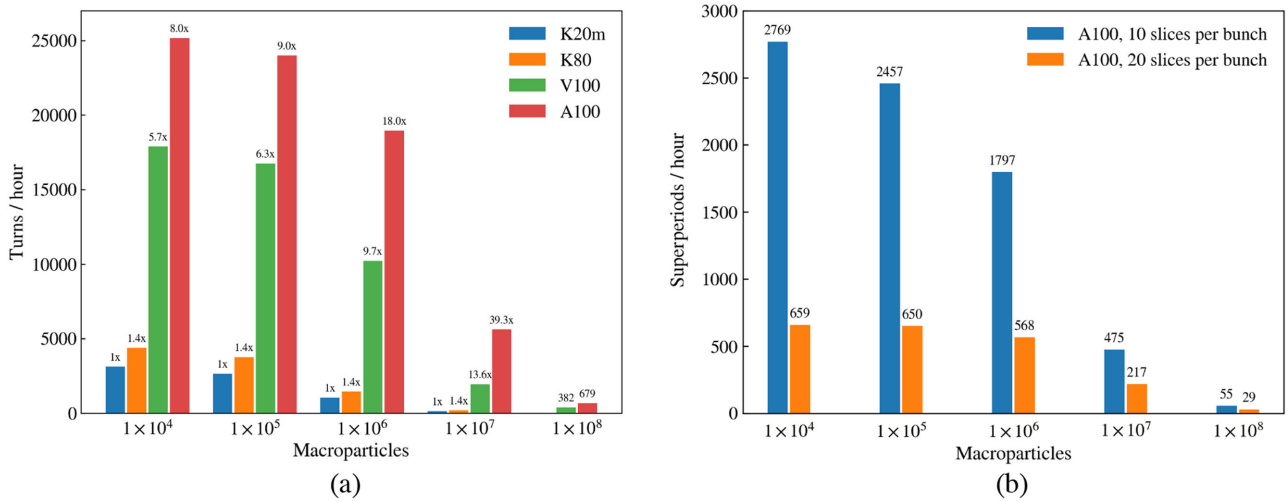

FIG. 3. Performance of the AthenaGPU program. (a) Computation speed on different GPUs in the 1e vs 1p mode with 10 slices per bunch. (b) Computation speed on A100 in the 8e vs 9p mode. Seventy-two collisions in one superperiod.

In the process of constructing the matrix, the circulant matrix will be used twice. In the polar coordinate system, the longitudinal phase space of the bunch is decomposed into N_r rings with the same number of particles, and each ring is equally divided into N_s parts, i.e., the longitudinal phase space is decomposed into $N_r N_s$ slices. Then the circulant matrix is used to perform synchrotron transport for each slice. The hourglass effect is introduced by calculating the beam-beam force of each slice at the collision point. When multiple bunches collide asymmetrically, the circulant matrix is used again to simplify the calculation. The circulant matrix can be used to rotate basic or nonbasic bunches, and both ways will lead to the same conclusion. In the case of rotating nonbasic bunches, the total matrix M_t can be expressed as

$$M_t = M_r \cdot M_k \cdot M_s \cdot M_\beta, \tag{10}$$

in which M_β is the betatron transfer matrix:

$$M_\beta = \begin{pmatrix} I(n_a) \otimes M(\nu_1) & 0 & 0 \\ 0 & I(n_b) \otimes M(\nu_2) & 0 \\ 0 & 0 & I(2n_c) \end{pmatrix}, \tag{11}$$

$$\begin{aligned} n_a &= N_{b_1} N_{r_1} N_{s_1}, \\ n_b &= N_{b_1} N_{r_2} N_{s_2}, \\ n_c &= (N_{b_2} - N_{b_1}) N_{r_2} N_{s_2}, \end{aligned} \tag{12}$$

where the subscripts 1 and 2 are used to indicate the properties of the basic and nonbasic beam, respectively, N_b is the bunch number, $I(n)$ is the identity matrix with $n \times n$ elements, $M(\nu)$ is the 2×2 one-turn matrix with betatron phase advance ν at the interaction point and $\otimes$ denotes the Kronecker product.

M_s is the synchrotron transfer matrix:

$$M_s = \begin{pmatrix} I(n_d) \otimes C_s(N_{s_1}) & 0 & 0 \\ 0 & I(n_e) \otimes C_s(N_{s_2}) & 0 \\ 0 & 0 & I(2n_f) \end{pmatrix}, \tag{13}$$

$$C_s(N_s) = P^{N_s \nu_s}(N_s) \otimes I(2), \tag{14}$$

$$\begin{aligned} n_d &= N_{b_1} N_{r_1}, \\ n_e &= N_{b_1} N_{r_2}, \\ n_f &= (N_{b_2} - N_{b_1}) N_{r_2} N_{s_2}, \end{aligned} \tag{15}$$

where ν_s is the synchrotron phase advance, $P(n)$ is the permutation matrix with $n \times n$ elements and can be expressed in two-line notation as

$$P = \begin{pmatrix} 1 & 2 & \cdots & n \\ n & 1 & \cdots & n-1 \end{pmatrix}. \tag{16}$$

M_k is the beam-beam kick matrix between all (N_{b_1}) bunches in the basic beam and the first N_{b_1} bunches in the nonbasic beam. Since each slice of the bunch has a corresponding longitudinal position, the real collision point CP between the slice j (basic bunch) and slice k (nonbasic bunch) involved in the collision can be calculated, as well as the distance l_j and l_k of these two slices relative to CP. The linearized beam-beam kick and drifts of the two slices are given by

$$M_{k,\text{slice}} = \begin{pmatrix} 1 & -l_j & 0 & 0 \\ 0 & 1 & 0 & 0 \\ 0 & 0 & 1 & -l_k \\ 0 & 0 & 0 & 1 \end{pmatrix} \cdot \begin{pmatrix} 1 & 0 & 0 & 0 \\ -\frac{4\pi\Xi_j}{N_{r_1} N_{s_1} \beta_j} & 1 & \frac{4\pi\Xi_j}{N_{r_1} N_{s_1} \beta_j} & 0 \\ 0 & 0 & 1 & 0 \\ \frac{4\pi\Xi_k}{N_{r_2} N_{s_2} \beta_k} & 0 & -\frac{4\pi\Xi_k}{N_{r_2} N_{s_2} \beta_k} & 1 \end{pmatrix} \cdot \begin{pmatrix} 1 & l_j & 0 & 0 \\ 0 & 1 & 0 & 0 \\ 0 & 0 & 1 & l_k \\ 0 & 0 & 0 & 1 \end{pmatrix}, \tag{17}$$

where β is the beta function at CP, and Ξ is the coherent beam-beam parameter of the bunch to which the slice belongs at CP. The Ξ of the basic bunch is given by

$$\Xi_{x,y} = \frac{N r_0 \beta_{x,y}}{2\pi\gamma\Sigma_{x,y}(\Sigma_x + \Sigma_y)} \tag{18}$$

where N is the number of particles in the nonbasic bunch, r_0, β, and γ are the classical particle radius, beta function, and relativistic factor of the basic bunch, and Σ is the effective bunch size calculated from the horizontal or vertical bunch size of the two bunches $\Sigma = \sqrt{\sigma_1^2 + \sigma_2^2}$. At the IP, Ξ is half of the nominal incoherent beam-beam parameter ξ. When the matrix dimension is expanded to include all slices, M_k is obtained by multiplying $M_{k,\text{slice}}$ between all slices in order of collision.

M_r is the matrix that rotates the nonbasic bunches to implement asymmetric collision:

$$M_r = \begin{pmatrix} I(2N_{b_1} N_{r_1} N_{s_1}) & 0 \\ 0 & C_r(N_{b_2}) \otimes I(2N_{r_2} N_{s_2}) \end{pmatrix}, \tag{19}$$

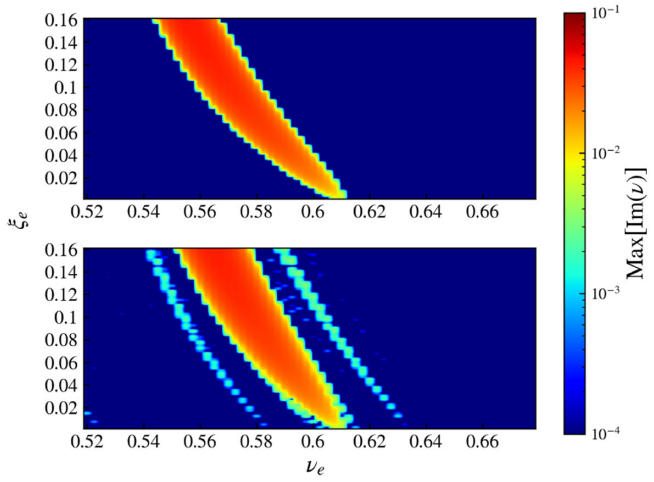

FIG. 4. The maximum value of the imaginary part of the eigentunes as a function of the horizontal ν_e and ξ_e in the 3e vs 5p mode. ν_p and ξ_p are 0.315 and 0.004, respectively. The longitudinal phase space is decomposed (bottom) or not (top). In the bottom figure, N_r and N_s are set to 5 and 33, respectively.

$$C_r(N_{b_2}) = P^{N_{b_2}-N_{b_1}}(N_{b_2}). \tag{20}$$

In the matrix model, we study the motion of the centroid of a slice or bunch, which means that this model can only account for dipole instability. Furthermore, the beam-beam force is linearized so that the nonlinear effects, such as Landau damping, are neglected. The matrix model can be used to take into account the crossing angle [19]. However, as already explained in Sec. II A 2, we assume no crossing angle in this paper and therefore do not discuss it.

Figure 4 illustrates the difference between the results when considering and not considering the longitudinal phase space decomposition in the 3e vs 5p mode. The horizontal ξ_p and ν_p of the proton bunch are set to 0.004 and 0.315, respectively, and then the horizontal ξ_e and ν_e of the electron bunch are scanned in steps of 0.0025. Solving for the matrix M_t in Eq. (10) yields multiple eigentunes, and the imaginary part of these eigentunes reflects the instability growth rate. The maximum value of the imaginary part of these eigentunes is plotted in Fig. 4. When considering the longitudinal phase space decomposition, the instability regions caused by the synchrotron oscillation of electron bunch can be observed on both sides of the central instability region, and the central instability region has covered the instability regions associated with the synchrotron oscillation of proton bunch.

III. INSTABILITY IN DIFFERENT COLLISION MODES

Assuming that there are N_1 bunches of beam 1 and N_2 bunches of beam 2, N_1 and N_2 are coprime. In the Fourier spectrum of the bunch centroid of beam 1, the tune ν_1 of beam 1 and the N_2 tunes ν_2^{eff} called effective tunes caused by beam 2 can be observed. This ν_2^{eff} is given by [4]

$$\nu_2^{\text{eff}} = \frac{N_1\nu_2 + i}{N_2}, \qquad i = 1, 2, \ldots, N_2. \tag{21}$$

It is clear that the number of effective tunes increases with the number of bunches. More effective tunes mean that the beam is more likely to enter the resonance region.

Figure 5 shows the horizontal spectrum of the electron bunch and proton bunch in the 4e vs 7p collision mode. Since the initial transverse distributions of the electron and proton bunches are Gaussian, their initial horizontal coherent frequencies are 0.624 and 0.317, respectively. In Fig. 5(a), vertical lines represent the positions of ν_p^{eff}

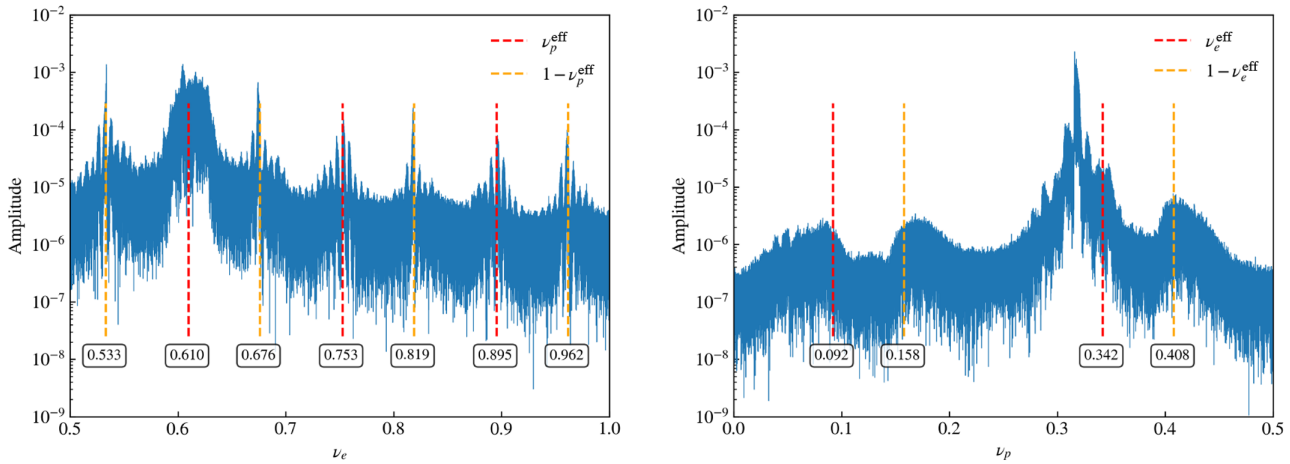

FIG. 5. In the 4e vs 7p collision mode, 1×10^5 superperiods are simulated using AthenaGPU. FFT algorithm is used to get the spectrum from the bunch centroid. The values of ν^{eff} and $1-\nu^{\text{eff}}$ are indicated in each figure. (a) The horizontal spectrum of an electron bunch. (b) The horizontal spectrum of a proton bunch.

and $1-\nu_p^{\mathrm{eff}}$ of the proton calculated by Eq. (21), the synchrotron sidebands of the proton also follow that formula. The differences between the amplitude of proton and electron frequencies are within an order of magnitude, which reflects the significant influence of the proton bunches on the electron bunches. In Fig. 5(b), the ν_e^{eff} of the electron bunch cannot be clearly distinguished because of its wide spectrum width, but the positions of each ν_e^{eff} in the spectrum are consistent with the theoretical values. Since the beam-beam force of the electron bunch has little effect on proton bunch, the amplitude of ν_e^{eff} is much smaller than that of ν_p, and the amplitude of $\nu_e^{\mathrm{eff}}=0.342$ is covered by the amplitude of ν_p and cannot be observed.

Four sets of simulations with different collision modes were performed to observe the instabilities caused by asymmetric collisions: 1e vs 1p, 2e vs 3p, 3e vs 5p, and 4e vs 7p. In all four collision modes, the collision frequency is 100 MHz, and the beam parameters and simulation parameters are the same, as shown in Tables I and II, respectively. The simulation results are shown in Figs. 6 and 7. Since the proton and electron beams are stable in the vertical direction in these four collision modes, only the evolution of the bunch centroid and bunch size in the horizontal direction is shown. In collisions where the number of bunches in both beams is asymmetric, all bunches in a beam behave the same, so only one of them is selected for demonstration. According to the simulation results, if the amplitude of the bunch centroid increases, then there is dipole instability, and if the amplitude of the bunch size increases, then there is quadrupole instability.

In the 1e vs 1p and 4e vs 7p collision modes, all bunches are stable, and the bunch states are the same. The same luminosities are achieved in both collision modes. Due to the dynamic beta effect driven by the beam-beam force of the proton bunch, the electron bunch size readjusts to a value lower than the design after dozens of turns, so the simulated luminosity is higher than the design value of $2.0\times10^{33}\ \mathrm{cm^{-2}\,s^{-1}}$.

TABLE II. The parameters for the simulation.

Parameter	Electron	Proton
Macroparticles per bunch	1×10^6	1×10^6
Number of grids (H/V)	512/512	
Grid size (H/V) (μm)	10/6	
Number of slices per bunch	20	5

In the 2e vs 3p mode, the electron and proton bunches show quadrupole instability at the beginning, while the centroids of all bunches are stable. Similar instabilities were already observed using a different model in Ref. [4]. After a certain number of turns, as the amplitude of the quadrupole oscillation gradually increases, the bunch centroid also begins to oscillate, i.e., dipole instability occurs. Although synchrotron radiation can suppress the increase of the electron bunch size, the proton bunch size still oscillates around a large value, which leads to a degradation of luminosity. Through simulations, it is found that the two beams will return to stability after adjusting the horizontal tune of the electron beam to 0.62.

In the 3e vs 5p mode, the electron and proton bunches show very strong coherent instability. The proton bunch has lost 0.1% of the macroparticles after 10×10^4 superperiods. A sum resonance between the electron and proton bunches can be observed from the matrix model. For the convenience of observation, N_r and N_s are both set to 1. Figures 8(a) and 8(b) show the eigentunes obtained by rotating electron (basic) bunches or proton (nonbasic) bunches in the matrix model, respectively. With the enhancement of the beam-beam effect, the two beams become unstable when the two frequencies merge

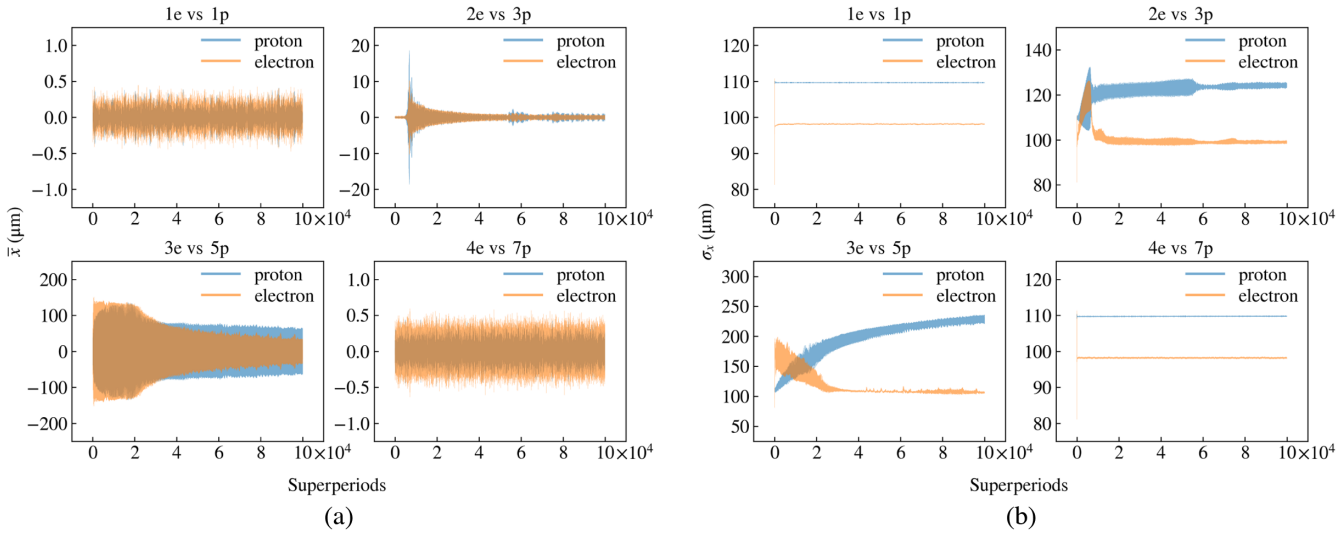

FIG. 6. Evolution of the horizontal centroid (a) and size (b) of the proton and electron bunches in different collision modes.

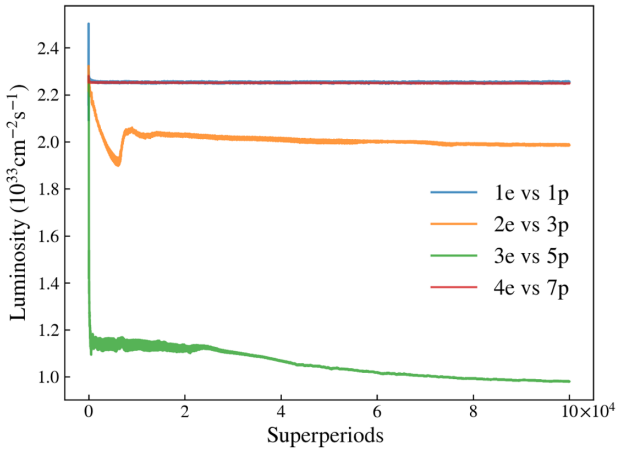

FIG. 7. Evolution of the luminosity in different collision modes.

($\xi_e = 0.054$), and the instability disappears when the frequencies are separated ($\xi_e = 0.13$). From the perspective of the electron beam, the resonance occurs between $\nu_e = 0.58$ and $\nu_p^{\text{eff}} = 0.389$. From the proton beam perspective, the resonance occurs between $\nu_p = 0.315$ and $\nu_e^{\text{eff}} = 0.633$. These two perspectives are actually equivalent, and they both correspond to the resonance of $N_1\nu_2 + N_2\nu_1 \sim$ integer.

In order to obtain the dipole instability region in the 3e vs 5p mode, the nominal tunes of the electron and proton beam are scanned in steps of 0.0025, and the maximum value of the imaginary part of the eigentunes is plotted in Fig. 9. Here, to consider the synchrotron oscillation and the hourglass effect in the matrix model, N_r and N_s are set to 5 and 33, respectively. It can be observed that the current tunes are located in a dipole instability region.

According to the instability region shown in Fig. 9, the instability can be avoided by moving ν_e to the area between the instability region associated with the synchrotron oscillation and the central instability region or to the area greater than 0.61, but the simulation results show that the beam does not become stable until increasing ν_e to 0.63. The reason for the discrepancy between the matrix results and the simulation results should be that the coherent frequency of the electron bunch is a fixed value in the matrix model, while the coherent frequency in the simulation is actually within a certain frequency range similar to Fig. 5(a). Through the spectrum of the electron bunch centroid, it can be concluded that the horizontal ξ_e is in the range of [0.04, 0.09]. In order to calculate the influence of the electron coherent spectrum width on the area of the instability region by the matrix model, the values of the imaginary part of the eigentunes in the above range of ξ_e are projected on the ν_e axis using the data from the bottom figure in Fig. 4, and the results are shown in Fig. 10. It can be observed that instability occurs at $\nu_e = 0.61$ and $\nu_e = 0.62$, which is consistent with the results observed in the simulations.

The above simulations show that asymmetric collision may destabilize the beams that are stable in symmetric collision mode and adjusting the nominal tunes is an effective way to avoid resonance.

IV. BEAM-BEAM LIMIT

In order to study the influence of asymmetric collision on the beam-beam limit, several simulations are performed in 1e vs 1p and 4e vs 7p modes with different bunch intensities while keeping other parameters constant, and the beam-beam limit is discussed by the luminosity relative degradation, which is given by

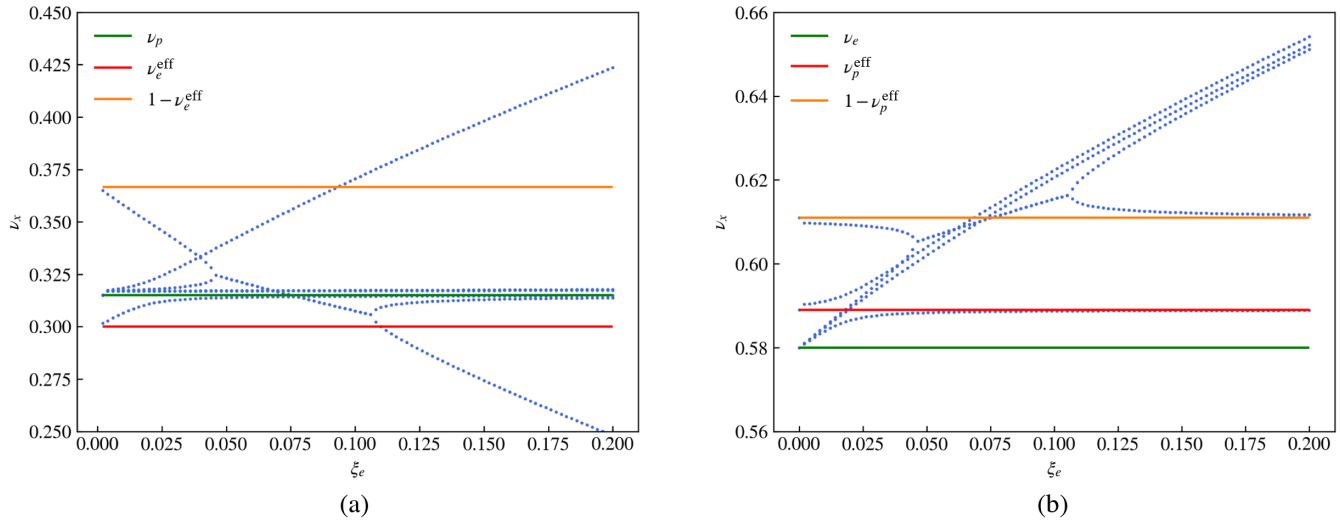

FIG. 8. The real part of the horizontal eigentunes in the 3e vs 5p mode. The matrix model is used to scan ξ_e in steps of 0.002 without considering the synchrotron oscillation and the hourglass effect. ξ_p is fixed at 0.004. (a) Rotating electron bunches in the matrix model. (b) Rotating proton bunches in the matrix model.

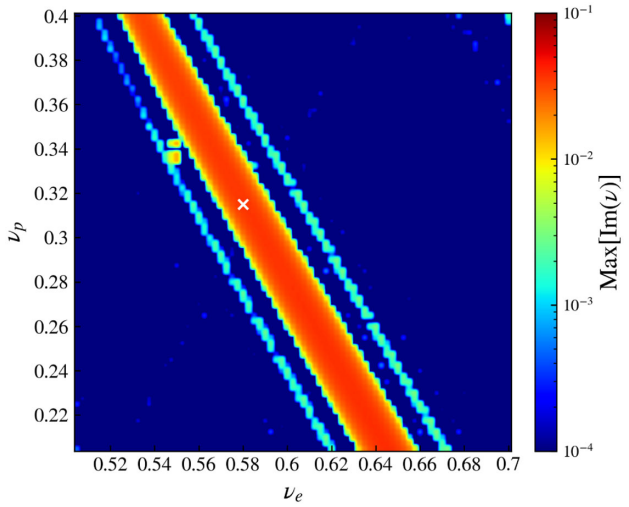

FIG. 9. The maximum value of the imaginary part of the eigentunes as a function of the horizontal ν_e and ν_p in the 3e vs 5p mode. ξ_e and ξ_p are 0.088 and 0.004, respectively. The cross indicates $\nu_e = 0.58$, $\nu_p = 0.315$.

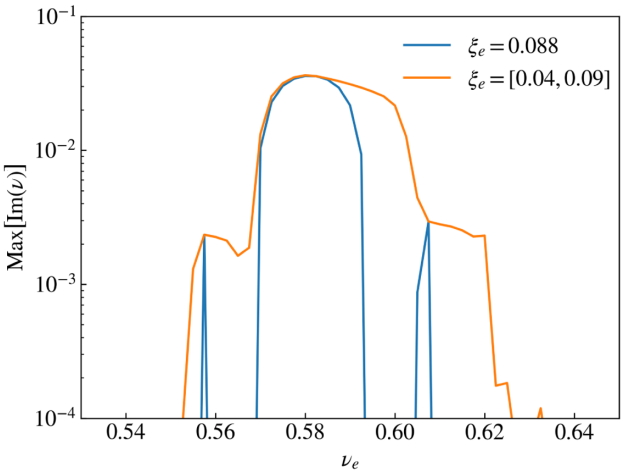

FIG. 10. Projection of the maximum value of the imaginary part of the eigentunes corresponding to ξ_e on the ν_e axis in the 3e vs 5p mode.

$$D_L = -\frac{L_{\text{final}} - L_{\text{init}}}{L_{\text{init}}}, \tag{22}$$

where L_{init} is the average luminosity of the 100th to 300th turns, L_{final} is the average luminosity of the last 200 turns. The first 100 turns are ignored to avoid errors introduced by large luminosity oscillations at the beginning of the collision.

For asymmetric collision, the sum of the luminosity acquired after one turn of all bunches in a beam is defined as the beam luminosity. Since the number of turns of the electron and proton bunches in asymmetric collisions is different, the choice of simulation turns in the 1e vs 1p mode is important for a fair comparison between the 1e vs 1p mode and the 4e vs 7p mode. When the beams are stable, the main contribution to the luminosity degradation is the increase of proton bunch size, so in this case, one should let the proton beams in both modes rotate the same number of turns for comparison. In contrast, when the beams are unstable, the instability dominates the degradation of luminosity. Therefore, letting the electron or proton beam rotate the same number of revolutions is fine.

In Fig. 11, 5×10^4 superperiods are simulated in the 4e vs 7p mode and 20×10^4 turns in the 1e vs 1p mode, and D_L is calculated from the luminosity of the proton beam. Figure 11(a) shows the effect of increasing electron bunch intensity on the D_L value. In the process of increasing the electron bunch intensity from $0.1N_{e_0}$ to $4N_{e_0}$, the electron

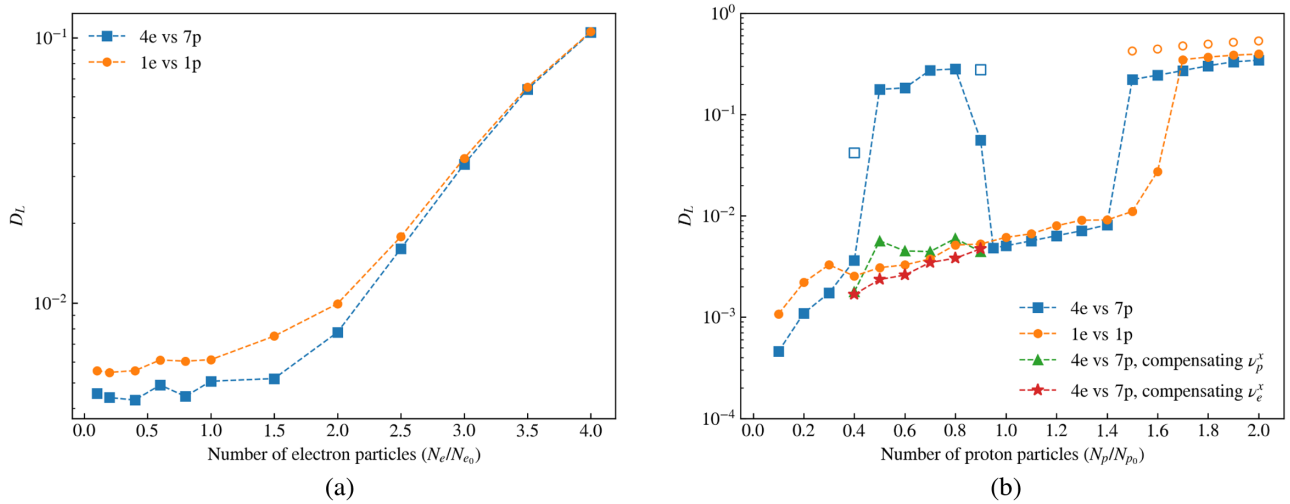

FIG. 11. D_L value as a function of electron bunch intensity (a) and proton bunch intensity (b) in 1e vs 1p and 4e vs 7p modes. N_e and N_p are the numbers of particles in each electron and proton bunch, respectively. N_{e_0} and N_{p_0} are the design parameters that have been listed in Table I.

and proton beams are always stable in both collision modes, and there is no change in the electron bunch size, while the proton bunch size keeps increasing, which is the main source of luminosity degradation. The simulation results show that the design intensity of the electron bunch can continue to increase without considering other effects. The growth of the proton bunch size can be suppressed by methods such as beam cooling to achieve higher luminosity. When N_e is less than or equal to $2N_{e_0}$, there is less luminosity degradation in the 4e vs 7p mode compared to the symmetric collision mode.

The D_L values obtained from the simulation at different proton bunch intensities are shown in Fig. 11(b). At some intensities, the two beams are always unstable within the preset number of turns, so more turns are simulated until the two beams reach equilibrium, at which point the D_L value is represented by a hollow circle (1e vs 1p) or hollow square (4e vs 7p).

When the proton bunch intensity decreases from the design value N_{p_0}, there is a significant luminosity degradation in the 4e vs 7p mode in the range of 0.4–0.9N_{p_0}, but not in the symmetric mode. Through the evolution of the bunch centroid and size, the beams show similar quadrupole instability in the horizontal direction within the above intensity range. To determine whether there is an instability region near the design tunes, the nominal tunes of the electron and proton beam were scanned. Taking the case of $N_p = 0.6N_{p_0}$ as a typical example, the D_L values from the self-consistent simulation are shown by different colors in Fig. 12. The arrows in Fig. 12 indicate the dipole and quadrupole instability regions obtained by analyzing the bunch states. It can be observed that the design tunes are located in a quadrupole instability region. Keeping the horizontal nominal tune of the proton beam constant, the simulation results of scanning the proton bunch intensity

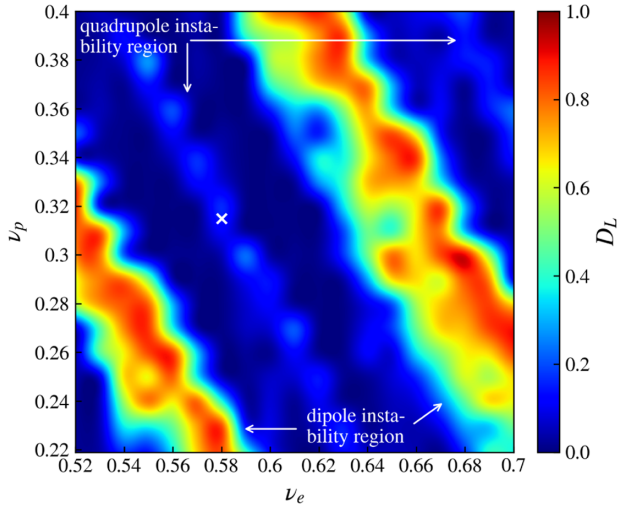

FIG. 12. D_L value as a function of the horizontal ν_e and ν_p in the 4e vs 7p mode. The cross indicates $\nu_e = 0.58$, $\nu_p = 0.315$.

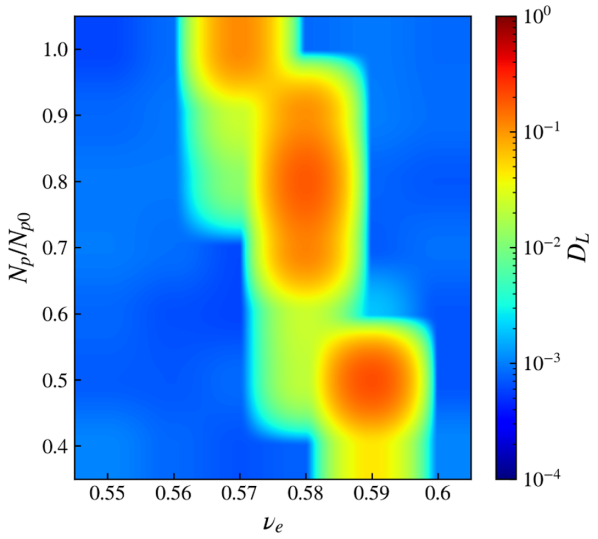

FIG. 13. D_L value as a function of the horizontal ν_e and proton bunch intensity in the 4e vs 7p mode.

and the horizontal nominal tune of the electron bunch are shown in Fig. 13. The scan step is 0.01, and the horizontal tune of the proton beam is 0.31 for the convenience of scanning. The region where the luminosity appears to be significantly degraded is the quadrupole instability region. It can be observed that the quadrupole instability region is shifting to the right as the proton bunch intensity decreases.

Based on the above results, the process of instability occurring in the 4e vs 7p mode when the proton intensity decreases from N_{p_0} can be explained visually using Fig. 14. When the proton intensity N_p is equal to N_{p_0}, the quadrupole instability region is indicated by the blue area, which is on the left side of the nominal tunes ν_1, and the beams are stable at this time. As N_p decreases, the quadrupole instability region shifts to the right. When N_p is in the

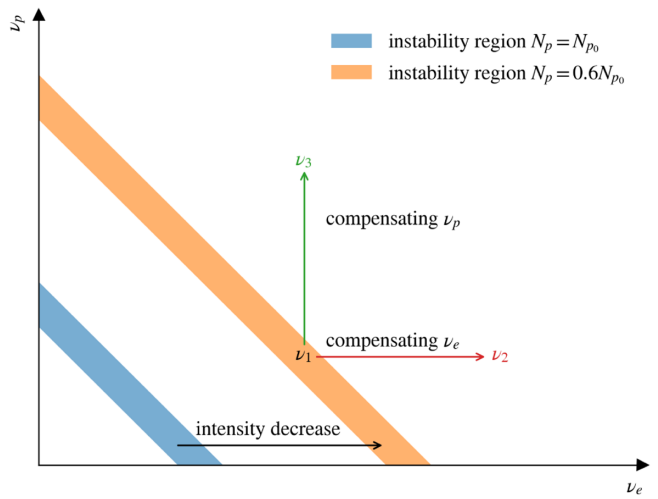

FIG. 14. Schematic diagram of the resonance region and measures for compensating the nominal tune.

range of 0.4–$0.9N_{p_0}$, ν_1 is located in the quadrupole instability region, and the beams become unstable, as shown by the orange area. When N_p is in the range of 0.1–$0.3N_{p_0}$, the quadrupole instability region no longer covers ν_1, and the beams return to stability. In order to keep the nominal tune ν_1 out of the quadrupole instability region when N_p is in the range of 0.4–$0.9N_{p_0}$, the horizontal nominal tune of the electron beam is compensated by a value equal to the change of coherent tune due to the decrease of the proton beam intensity, and the nominal tune after compensation is denoted by ν_2. This process is shown by the red arrow. In addition, attempts are made to avoid instability by compensating for the horizontal nominal tune of the proton beam, as shown by the green arrow and ν_3.

The values of ν_e and ν_p after compensation are listed in Table III. The D_L values using the compensated ν_e are shown as red stars in Fig. 11(b), indicating that the luminosity degradation is significantly reduced after the ν_e is compensated. The bunch size data show that instability does not appear. The green triangles in Fig. 11(b) represent the D_L values after compensating for ν_p. Although the effect is not as good as compensating for ν_e, compensating for ν_p still reduces the luminosity degradation and stabilizes the beams in the intensity range of 0.4–$0.9N_{p_0}$.

When the proton bunch intensity increases from the design value N_{p_0} to $1.5N_{p_0}$, there is significant luminosity degradations in both collision modes and dipole instability appears in the horizontal direction. The beam-beam parameter and nominal tune of the electron beam in the horizontal direction are scanned using the matrix method, and the scanning results are shown in Fig. 15. When the beam-beam parameter of the electron beam is increased to about 0.14, that is, the proton bunch intensity is $1.59N_{p_0}$, the nominal tune enters the dipole instability region associated with the synchrotron oscillation, and dipole instability appears, which is consistent with the simulation results with a small deviation.

TABLE III. The horizontal tunes after compensation.

N_p/N_{p_0}	0.4	0.5	0.6	0.7	0.8	0.9
ν_e	0.6064	0.602	0.5976	0.593	0.5888	0.5844
ν_p	0.42	0.39	0.38	0.3527	0.335	0.3227

V. IMPACT OF A RAPID DISTURBANCE

The eRing and pRing of EicC may adopt a full-energy injection scheme, so the injection kicker may rapidly and drastically change the orbit of a bunch, resulting in an offset between the transverse position of the bunch at the collision point relative to its ideal position. When a bunch has a transverse offset at the collision point, it will show coherent motion and may become unstable. In order to study the impact of such kind of offset collision in symmetric and asymmetric collision modes, simulations are performed without considering the intervention of the feedback system. A horizontal offset Δx is added to all particles in the bunch generated at the collision point at the beginning of the simulation. For the electron bunch, even if its horizontal offset reaches $15\sigma_x$, the synchrotron radiation will still damp its coherent oscillation, and the luminosity will return to approximately the same value without the offset, as shown in Fig. 16. Therefore, we only study the case where the proton bunch has a horizontal offset.

In the 1e vs 1p mode, the proton beam becomes unstable when Δx increases to $0.4\sigma_x$. The orange lines in Fig. 17

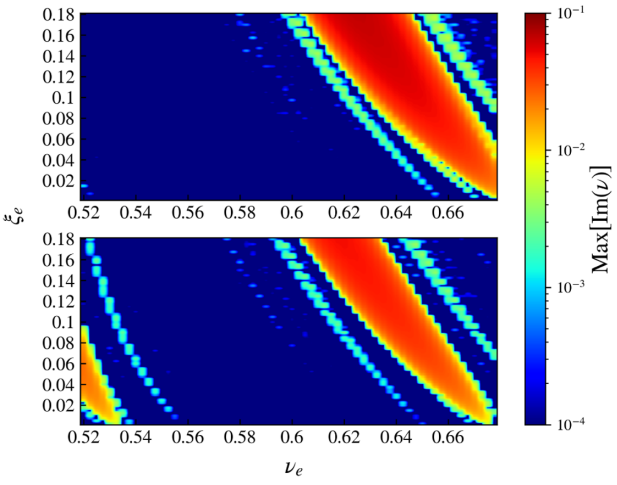

FIG. 15. The maximum value of the imaginary part of the eigentunes as a function of the horizontal ν_e and ξ_e in 1e vs 1p (top) and 4e vs 7p (bottom) modes. ν_p and ξ_p are 0.315 and 0.004, N_r and N_s are 5 and 33.

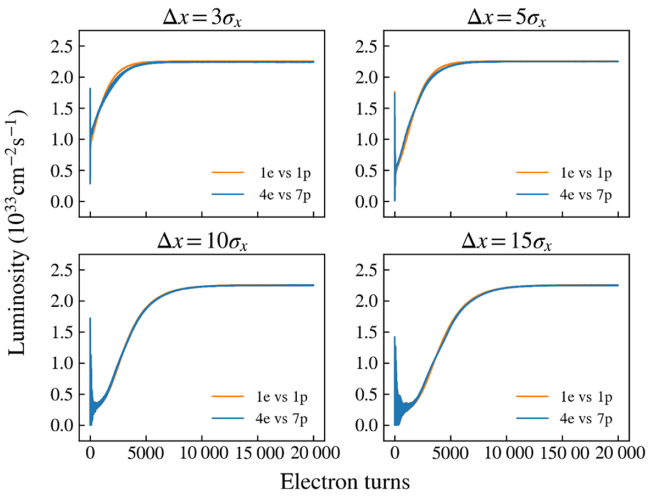

FIG. 16. Luminosity for various horizontal offsets Δx of the electron beam. In the 4e vs 7p collision mode, all four electron bunches have the same Δx.

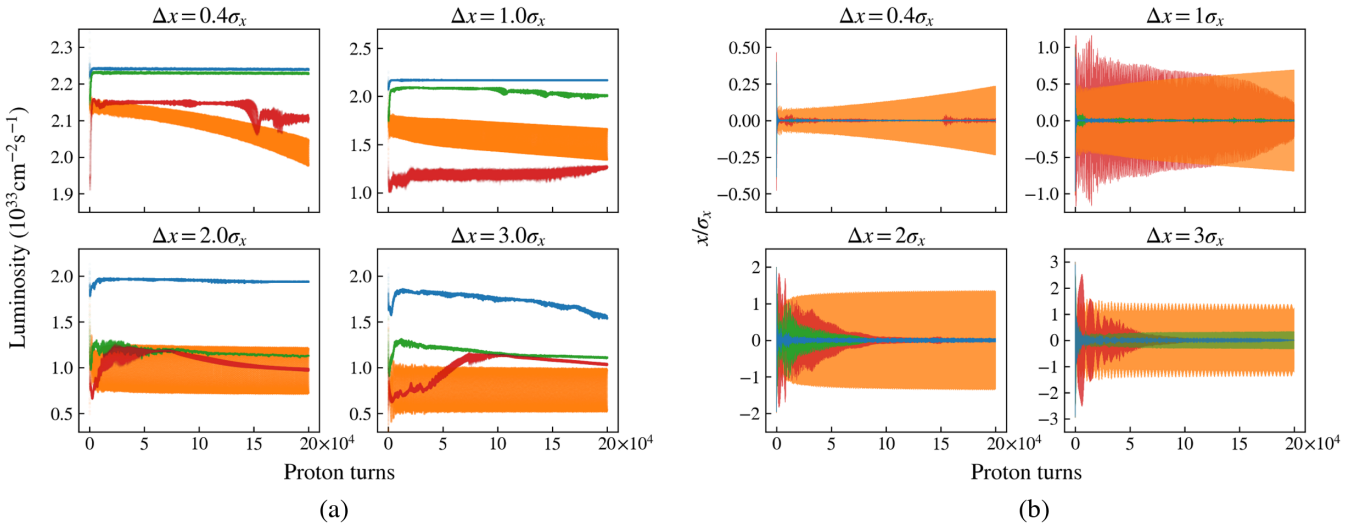

FIG. 17. The orange color represents the 1e vs 1p collision mode. The blue, green, and red colors represent that 1, 2, and all 7 proton bunches are displaced in the 4e vs 7p collision mode, respectively. (a) Luminosity for various horizontal offsets Δx of the proton beam. (b) Evolution of the centroid of the displaced proton bunch for various horizontal offsets Δx.

show the evolution of the luminosity and the centroid of the proton bunch in this collision mode. As Δx increases, the coherent motion of the displaced proton bunch becomes stronger without any sign of decoherence. In the case when only one proton bunch is displaced in the 4e vs 7p mode, the instability threshold and luminosity are higher than that of the 1e vs 1p mode, as shown by the blue lines in Fig. 17. When Fourier spectrum analysis is performed on statistical data such as bunch size or emittance of the electron bunch, the frequencies of $1/7$ and its multiples can be observed. This is because the electron bunch does not encounter the displaced proton bunch in every turn but collides with it at a fixed frequency. As the number of displaced proton bunches in the 4e vs 7p mode increases, the maximum allowable offset while the beam remains stable decreases. When all proton bunches are displaced, the maximum allowable offset is the same as that of the 1e vs 1p mode. It can be observed from Fig. 17(b) that the decoherence of the displaced proton bunch is faster in the 4e vs 7p mode than in the 1e vs 1p mode.

As shown in Fig. 17(b), all simulated offsets of the displaced proton bunch are large enough to cause instability in the 1e vs 1p mode. In the 4e vs 7p mode, the displaced proton bunch also drives the electron bunch and causes instability, and the electron bunch continues to interact with other proton bunches. Eventually, the impact caused by the offset collision is transmitted to all bunches in both rings after one superperiod. However, the motions of all but the displaced proton bunch are stable, so the asymmetric collision mode takes longer than the symmetric collision mode for all the bunches to become unstable. The more undisplaced bunches in the beam, the faster the displaced bunch will be decoherent. Regardless of the collision mode, if the decoherence time is less than the instability growth time, the final result is that the instability is suppressed, otherwise, the instability appears.

VI. CONCLUSION

We developed a linear analysis program and a particle tracking program to study the asymmetric beam-beam effect in EicC.

The self-consistent simulations of different collision modes verify the conclusion in Ref. [4] that the resonances introduced by the asymmetric collision will lead to instabilities such as dipole instability and quadrupole instability. These resonances can be avoided by adjusting the nominal tunes, but if the beam-beam parameter is large or the resonance regions are dense, the nominal tunes adjustment may fail, and then the collision mode or beam parameters have to be changed.

The luminosity degradation at different bunch intensities in 1e vs 1p and 4e vs 7p modes indicate that the same luminosity can be achieved when the beams are stable in both collision modes. In the 4e vs 7p mode, instability is observed when the proton beam intensity decreases from the nominal value to a certain range. This means that although the beam is stable at the design parameters, instability may occur if the coherent frequency is shifted due to particle loss or other reasons. Therefore, when choosing the nominal tunes, in addition to avoiding the resonance region caused by asymmetric collision, a certain margin should be reserved to deal with the potential instability.

After adding a horizontal offset to the bunch to introduce coherent motion, the simulation results show that for a proton beam with weak radiation damping, the decoherence time of the displaced bunch is shorter in the

asymmetric collision mode than in the symmetric collision mode. The more undisplaced bunches in the beam, the faster the displaced bunch will be decoherent.

In conclusion, when only the beam-beam effect is considered, the simulation and calculation results in this paper show that the asymmetric collision mode is promising for EicC.

ACKNOWLEDGMENTS

Thank the support from the National Science Fund for Distinguished Young Scholars (No. 11825505), the National Key R&D Program of China (Grant No. 2019YFA0405400), and the National Natural Science Foundation of China (No. 12005274).

[1] D. P. Anderle, V. Bertone, X. Cao, L. Chang, N. Chang, G. Chen, X. Chen, Z. Chen *et al.*, Electron-ion collider in China, Front. Phys. **16**, 64701 (2021).

[2] J. C. Yang *et al.*, High Intensity Heavy Ion Accelerator Facility (HIAF) in China, Nucl. Instrum. Methods Phys. Res., Sect. B **317**, 263 (2013).

[3] K. Hirata and E. Keil, Barycentre motion of beams due to beam-beam interaction in asymmetric ring colliders, Nucl. Instrum. Methods Phys. Res., Sect. A **292**, 156 (1990).

[4] Y. Hao, V. N. Litvinenko, and V. Ptitsyn, Beam-beam effects of gear changing in ring-ring colliders, Phys. Rev. ST Accel. Beams **17**, 041001 (2014).

[5] J. Qiang, M. A. Furman, and R. D. Ryne, A parallel particle-in-cell model for beam-beam interaction in high energy ring colliders, J. Comput. Phys. **198**, 278 (2004).

[6] Y. Zhang, K. Ohmi, and L. Chen, Simulation study of beam-beam effects, Phys. Rev. ST Accel. Beams **8**, 074402 (2005).

[7] T. Pieloni, A study of beam-beam effects in hadron colliders with a large number of bunches, Ph.D. thesis, Ecole Polytechnique, Lausanne2008.

[8] cuFFT Library User's Guide (2022).

[9] CUDA C++ Programming Guide (2022).

[10] Y. K. Batygin, Particle-in-cell code beampath for beam dynamics simulations in linear accelerators and beamlines, Nucl. Instrum. Methods Phys. Res., Sect. A **539**, 455 (2005).

[11] W. JOHO, Representation of beam ellipses for transport calculation, Paul Scherrer Institute, Technical Report No. SIN-REPORT TM-11-14, 1980.

[12] K. Hirata, Analysis of Beam-Beam Interactions with a Large Crossing Angle, Phys. Rev. Lett. **74**, 2228 (1995).

[13] K. Hirata, H. Moshammer, and F. Ruggiero, A symplectic beam-beam interaction with energy change, Part. Accel. **40**, 205 (1993).

[14] M. A. Furman, Hourglass effects for asymmetric colliders, in *Proceedings of the 1991 Particle Accelerator Conference, San Francisco, CA, 1991* (IEEE, New York, 1991), p. 422.

[15] K. Ohmi, M. Tawada, Y. Cai, S. Kamada, K. Oide, and J. Qiang, Luminosity limit due to the beam-beam interactions with or without crossing angle, Phys. Rev. ST Accel. Beams **7**, 104401 (2004).

[16] C. K. Birdsall and D. Fuss, Clouds-in-clouds, clouds-in-cells physics for many-body plasma simulation, J. Comput. Phys. **135**, 141 (1997).

[17] K. Ohmi, Simulation of beam-beam effects in a circular e^+e^- collider, Phys. Rev. E **62**, 7287 (2000).

[18] S. White, X. Buffat, N. Mounet, and T. Pieloni, Transverse mode coupling instability of colliding beams, Phys. Rev. ST Accel. Beams **17**, 041002 (2014).

[19] X. Buffat, Transverse beams stability studies at the Large Hadron Collider, Ph.D. thesis, Ecole Polytechnique, Lausanne (2015).